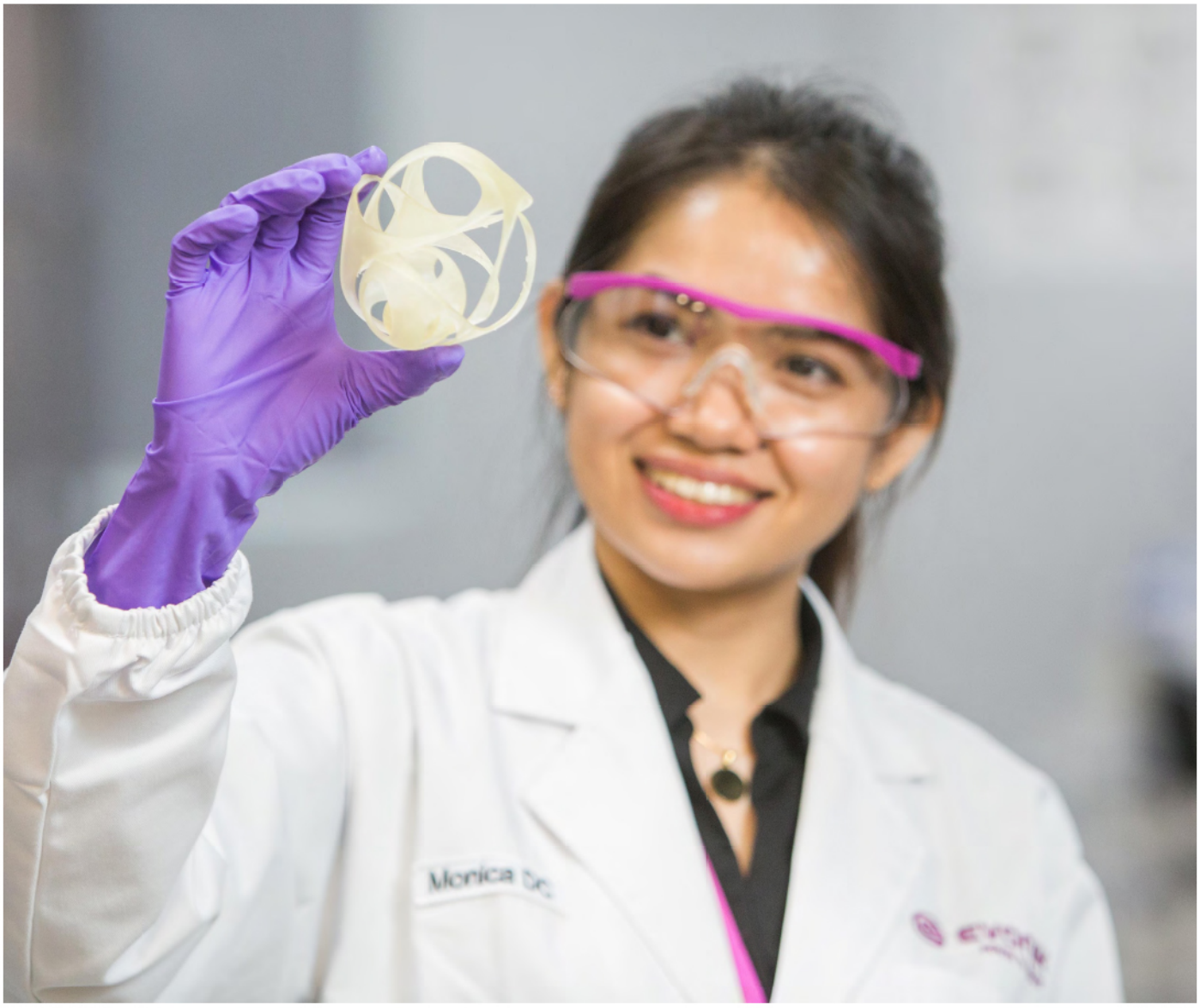

Pushing the boundaries of chemistry? It takes #HumanChemistry

Make your curiosity and talent as a chemist matter to the world with a specialty chemicals leader. Together, we combine cutting-edge science with engineering expertise to create solutions that answer real-world problems. Find out how our approach to technology creates more opportunities for growth, and see what chemistry can do for you at:

evonik.com/career

EVONIK
Leading Beyond Chemistry

ADVANCED FUNCTIONAL MATERIALS
www.afm-journal.de

Multifunctional Metamaterials for Energy Harvesting and Vibration Control

Xianchen Xu, Qian Wu, Yaokun Pang, Yuteng Cao, Yuhui Fang, Guoliang Huang, and Changyong Cao**

Multifunctional metamaterials (MFMs) capable of energy harvesting and vibration control are particularly attractive for smart structures, wearable/biointegrated electronics, and intelligent robotics. Here, a novel MFM based on triboelectric nanogenerators (TENGs), which can harvest environmental energy and reduce vibration simultaneously, is reported. The unit cells of the MFM consist of a local resonator, an integrated contact- separation mode TENG, and spiral-shaped connecting beams. A multiphysics theoretical model is developed for quantitatively evaluating the performance of the MFM by including the mechanical and electrical fields interactions, which is further validated by experimental testing. It is demonstrated that the TENG-based MFM can not only effectively harvest vibration energy to power electronics but also dramatically suppress low-frequency mechanical vibration. This work provides a new design and model for developing novel TENG-based MFMs for advanced smart systems used in a variety of applications.

1. Introduction

Metamaterials are engineered materials that have unique material characteristics such as negative refractive index or negative effective properties that cannot be observed in nature.[1,2] They have periodic or non-periodic architectured structures with single or multiple kinds of materials for structural (e.g., topological morphing, elastic wave, and vibration manipulation) and nonstructural functions (e.g., optical, acoustic, and electric control).[3–6] A combination of diffident kinds of functionality enables multifunctional metamaterials (MFMs) that can be used for a variety of applications in which the materials or structures need to simultaneously perform two or more functions.[7] For example, stimuli-responsive acoustic metamaterials were fabricated to tune negative-modulus and cavity-induced negative density with remote magnetic fields.[8] The tunable metamaterials were demonstrated as acoustic switch devices that can turn on and off acoustic transportation with various remote stimuli. Also, by introducing a flexible piezoelectric patch, a membrane-type acoustic metamaterial was developed for low-frequency sound insulation and energy harvesting from sound waves.[9] The dual functionality of the metamaterial device was further validated by experimental results, which show an over 20 dB sound transmission loss and a maximum energy conversion efficiency up to 15.3% simultaneously.

One promising engineering application of mechanical metamaterials is to prevent unwanted noises and/or vibrations in the low-frequency range.[10–13] It was found that a great amount of mechanical energy goes in and out of the local resonators in a cyclic manner, which means the trapped mechanical energy localizes in internal microstructural elements in the form of an oscillatory motion. Therefore, to develop a new multifuncational metamaterial capable of effectively reducing the vibration and simultaneously harvesting the trapped mechanical energy for practical application attracts long-standing attention over the years.[14,15] It is promising to use local microstructures, such as periodically distributed local resonators at a scale much less than the relevant wavelength, on a host plate to design such kind of multifunctional materials.[5,10,12] Four different kinds of energy harvesting mechanisms, i.e., electromagnetic [16,17] magnetoelectric,[18] piezoelectric,[19,20] and triboelectric,[21–26] have been widely explored to convert environmental energy to electrical energy under different conditions.

In comparison with the other three methods, a triboelectric nanogenerator (TENG) has a simpler structure but higher efficiency. It is based on the conjunction of triboelectrification effect and electrostatic induction and can efficiently harvest

X. Xu, Y. Pang, Y. Fang, C. Cao
Laboratory for Soft Machines and Electronics
Michigan State University
East Lansing, MI 48824, USA
E-mail: ccao@egr.msu.edu
Q. Wu, G. Huang
Department of Aerospace and Mechanical Engineering
University of Missouri
Columbia, MO 65211, USA
E-mail: huangg@missouri.edu
Y. Cao
Department of Civil and Environmental Engineering
Massachusetts Institute of Technology
Cambridge, MA 02139, USA
C. Cao
Departments of Mechanical Engineering
Electrical and Computer Engineering
Michigan State University
East Lansing, MI 48824, USA

The ORCID identification number(s) for the author(s) of this article can be found under https://doi.org/10.1002/adfm.202107896.

DOI: 10.1002/adfm.202107896

mechanical energy with different kinds of working modes: vertical contact mode,[27] lateral sliding mode,[28] freestanding mode,[29] and single-electrode mode.[30] Since its invention, researchers have proposed various approaches and novel designs to improve energy harvesting efficiency.[23] For instance, Wu et al. introduced a spring-based amplifier and coupled two picking-up vibration structures in the TENGs to improve the vibration energy harvesting efficiency at low frequencies.[31] Niu et al. proposed a theoretical model and derived an analytical relationship for a lateral sliding-mode TENG.[27] Based on this theoretical model, Salauddin et al. designed a hybrid energy harvester to harvest human-induced vibration energy.[32] Yang et al. also demonstrated a sliding-mode TENG to power a sensor that could detect the speed along one direction.[33]

In this article, we propose a new MFM capable of energy harvesting and vibration control based on the TENG technology. The unit cell of the metamaterial consists of a mass resonator, an integrated contact-separation mode TENG, and spiral-shaped connecting beams between the resonator and base. A multiphyiscs theoretical model is constructed to analyze the performance of the MFM by considering both mechanical and electrical fields. The effects of the key parameters: geometric dimension, structural configurations, and material properties on the performance of the MFM are numerically and experimentally investigated under different excitation frequencies. We demonstrate that our TENG-based MFM can effectively harvest vibration energy, significantly suppress the vibration and elastic wave mitigation, and even identify the frequency. The proposed advanced smart systems could be used for a variety of applications in automobiles, robotics, and implant devices.

2. Results and Analysis

2.1. Concept Design and Fabrication of the MFM

As shown in **Figure 1**a, the MFM consists of a series of unit cells based on TENGs and a supporting substrate made of acrylate. The unit cell (12 × 12 mm) is designed to be a chiral beam-like structure with a central mass connected (Figure 1b). The adoption of the chiral structure of beams is to maximize the effective contact area with the substrate in vibration. The central mass is 3D printed using nylon and coated a thin layer of aluminum (Al) film/foil on its back to serve as the electrode (Figure 1c).

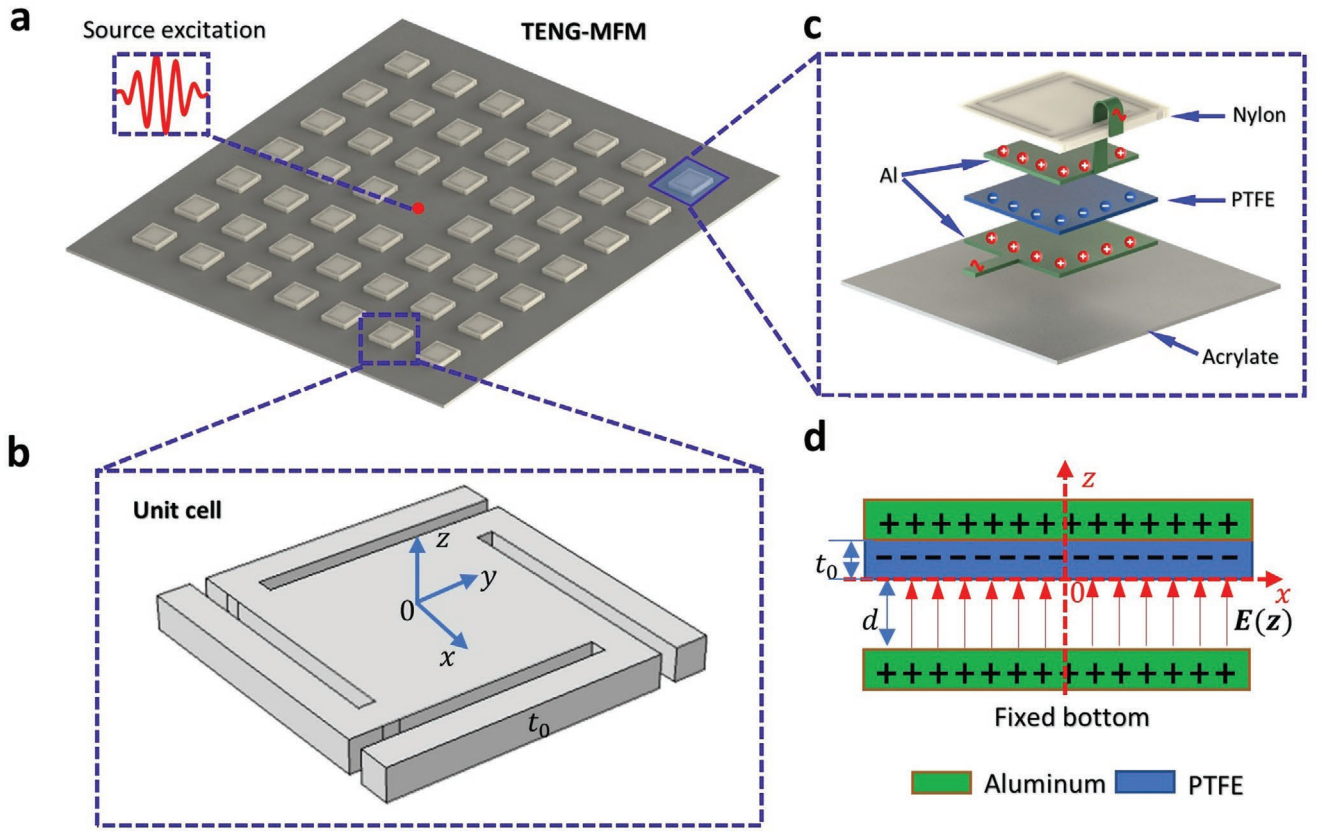

Figure 1. Proposed triboelectric nanogenerator (TENG) based multifunctional metamaterial (MFM). a) Schematic illustration of the TENG-MFM consisting of an array of structural TENG-based resonators. An external vibration load or acoustic wave is applied at the center of the TENG-MFM plate. b) Geometry of the unit cell resonator which has a central mass and connected with the base using chiral shape beams. c) Schematic illustration of the layered structure for the unit cell. The resonator is 3D printed using nylon, and then coated a thin layer of aluminum (Al) as electrode. The base is fabricated with acrylate plate and coated with a thin layer of Al before depositing another thin PTFE film on top of it. d) Schematic illustration of the working mechanism of the contact-separate mode TENG. An electric field $E(z)$ will be formed and varying with the charge volume and gap distance d when indued charges appear on the Al and PTFE surface.

Another thin layer of Al film is coated on the top surface of the acrylate plate, following a pattern defined based on the position and size of the central mass. After that, a thin polytetrafluoroethylene (PTFE) film is deposited onto the Al film of the substrate surface (Figure 1c). A small gap between the mass resonator and the bottom substrate is designed to allow the vibration motions of the central mass when an external excitation is applied. Owing to the different attraction abilities to electrons by different triboelectric materials,[21,27] the cyclic contact-separation interactions between the Al and PTFE layers will generate electrical charges (Figure 1d) and will also affect the vibrations of the central mass due to the induced electrostatic force. In addition, the variation of the vibration frequency and amplitude will result in the change of the output voltage/current, making it possible to serve as a vibration sensor for external mechanical excitations nearby the TENG-MFM.

2.2. Multiphysics Theoretical and Numerical Models of the MFM

As shown in Figure 1b, the unit cell of the MFM has four sets of connecting beams and each set has one or more segments where the first segment is perpendicularly connected with the next one (counting from outside to inside). The last connecting segment of each beam is bonded with a rectangular plate, which can be simplified as a central mass (Figure S1, Supporting Information). Since the central mass vibrates when subjected to an external excitation, it will lead to the possible contact between the nylon resonator and the base plate. If we substitute the connecting beams with an equivalent spring and a damper, we can obtain a dynamic model for the unit cell, as shown in **Figure 2**a, where a movable mass m_1 interacts with a rigid base using a linear spring with a stiffness constant of k and a viscous damper with a damping coefficient of c. As a result, when the base is excited by a load $w_b(t) = A_0 e^{i\omega t}$, where A_0 is excitation amplitude and ω is the corresponded frequency, the governing equation for the Euler–Bernoulli beam can be given as[34,35]

$$EI\frac{\partial^4 w_i(x,t)}{\partial x^4} + \rho A\frac{\partial^2 w_i(x,t)}{\partial t^2} = 0 \quad i = 1,2 \tag{1}$$

where t is the time, x is the axis along the length of the beam, i is the number of beams, E, I, ρ, A are Young's modulus, moment of inertia, mass density, and cross-section area of the beam, respectively. A rigid dam-board is placed under the mass with gap d to confine the vibration motion of the central mass, which is connected with the base plate by a linear spring k_d to represent the contact stiffness. From Equation (1), the equivalent spring constant can be calculated as

$$k = \frac{A_0}{\left(1 - m\omega^2\right)\sum_{j=1}^{4} A_{2j} e^{s_{2j} l_2}} \tag{2}$$

Therefore, the governing equation of the vibration system can be expressed as

$$m\ddot{w}_1 + c\dot{w}_1 + k \quad w_1 = F_b + F_e\left(w_1 - w_b > -d\right) \tag{3}$$

$$m\ddot{w}_1 + c\dot{w}_1 + \left(k + k_d\right) \quad w_1 = F_d + F_e\left(w_1 - w_b \le -d\right) \tag{4}$$

where $F_b = kw_b$, $F_d = (k + k_d)w_b$, $w_b = A_0 e^{i\omega t}$ is the excitation applied on the base plate, and F_e is the electrostatic force induced by the TENG, which can be calculated by[36,37]

$$F_e = \frac{a_0^2\sigma^2}{2\pi^2\varepsilon_0\varepsilon_\alpha\left(z_0 + d_0 + t_0\right)^2}\left\{\arctan\left[\frac{1}{4\left(z_0 + d_0 + t_0\right)\sqrt{\frac{1}{2} + \left(z_0 + d_0 + t_0\right)^2}}\right]\right\}^2 \tag{5}$$

The details for the calculations are presented in the Supporting Information.

Figure 2b shows the numerical results of the theoretical model of the unit cell with $k_d/k = 1$, $k_d/k = 5$, and $k_d/k = 10$, where the input frequency is 148 Hz and d is 2 mm. It is noted that if k_d is close to k, the contact will be a kind of soft touch, thereby the vibration of the mass m_1 looks more like a double spring parallel system, and the vibration is periodically symmetric. As $k_d >> k$, the contact surface becomes rigid, the lower valleys become sharper than the upper peaks, which indicates the contact/collision time becomes shorter. In this model, we only consider the elastic collision without energy conversation/dissipation although partial inelastic collision may occur in the process. This is because with high-frequency external excitation and suitable gap size between the substrate and mass resonator, the inelastic collision part is very small and has negligible effect on the dynamic responses of the resonator.

To verify the proposed model, we conduct a combined finite element (FE) analysis for the unit cell of TENG-MFM by using the Multiphysics COMSOL software package (Figure 2c), where the nonlinear spring constant is assumed to be $k_d/k = 20.62$. The simulation and theoretical results with a contact distance of $d = -2$ mm are in good agreement. Thus, the proposed numerical model can be used to study the TENG-MFM vibration. The vibration displacements of the central mass at peak (State I) and valley (State II) points are uniform and the displacement at the maximum negative amplitude has been constrained (Figure 2d). As expected, the stress and strain concentrations occur in the deformed beams, and there are small uniform stresses distributed on the central resonator (Figure S4, Supporting Information), indicating that designed TENG-MFM can achieve a nearly parallel contact-separate mode at the resonant frequency.

We further investigate the wave dispersion relations and vibration suppression performance of the proposed TENG-MFM using FE simulations. Figure 2e shows the unit cell with a lattice width of 40 mm in an MFM-TENG plate, where a plane stress assumption is used for the analysis. Figure 2f illustrates the corresponding reciprocal lattice vector for the MFM-TENGs. With prescribed periodic boundary conditions on the unit cell, we can obtain the dispersion diagrams for all the four different configurations (Figure 2g), which clearly exhibit a complete bandgap to lower frequencies (≈185 Hz). The shape of the first mode at 185 Hz is presented in the inset of Figure 2g. This bandgap is created by the local resonant mechanism because the wave speed in First Brillouin Zone (FBZ) along $\Gamma - X$ direction is close to zero. It indicates that the new TENG-MFM is

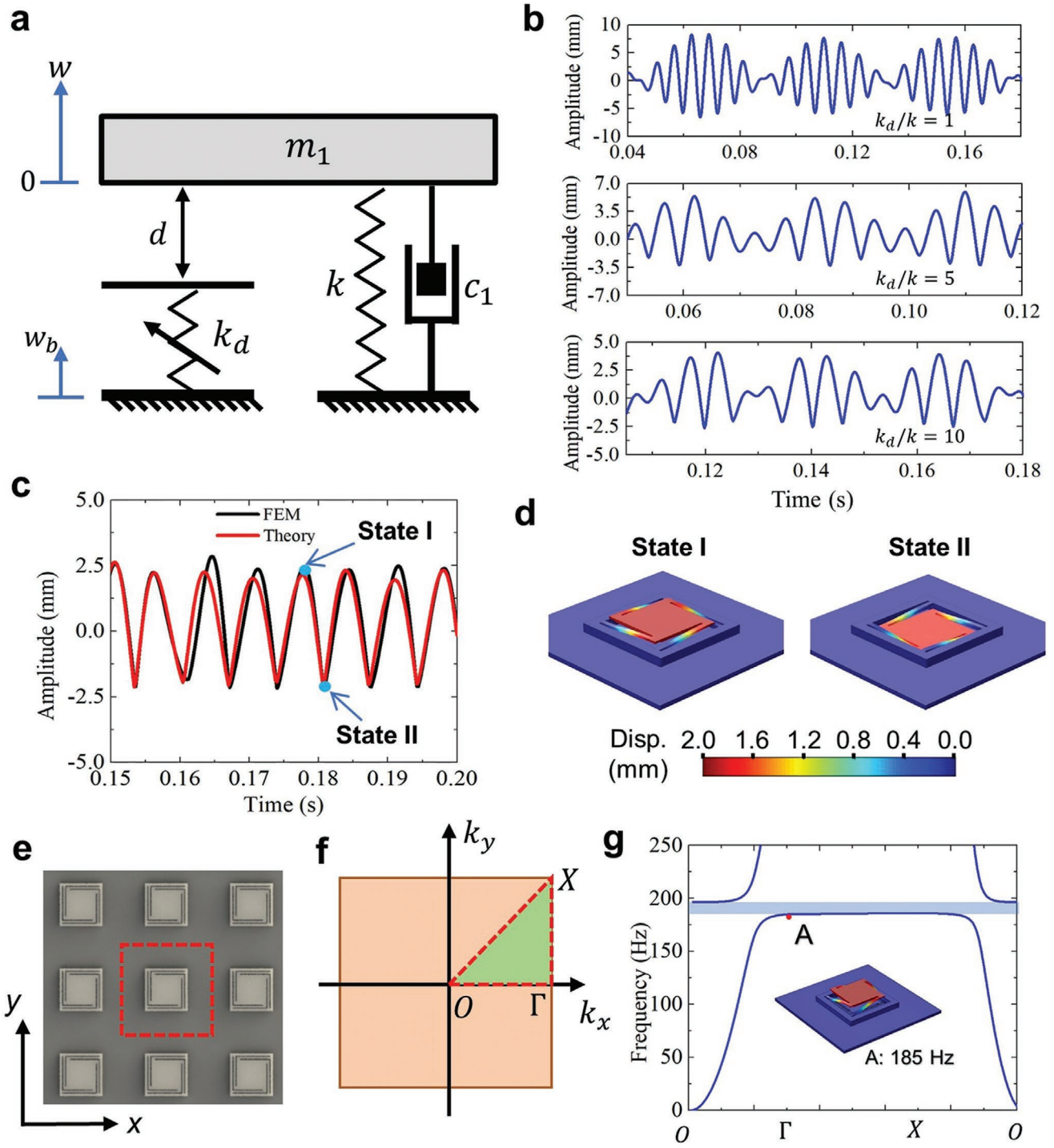

Figure 2. Mechanical vibration model and properties of the unit cell of triboelectric nanogenerator multifunctional metamaterial (TENG-MFM). a) Schematic diagram of the vibration model. The 3D printed nylon layer is treated as a concentrated mass m_1. The connection beams between the central mass and base are simplified as a linear spring with a constant of k and the damping parameter is assumed to be c_1. The collision or contact between the nylon layer and the polytetrafluoroethylene (PTFE) coating is dealt with a spring k_d. The initial vibration gap without contacting the bottom layer is set to be d so that the effective mass can oscillate with amplitude w by the excitation from the base with an amplitude of A_0. b) The dynamic responses of the mass m_1 in time-domain when the parameter in the model is $k_d/k = 1$, $k_d/k = 5$, and $k_d/k = 10$ under the excitation of $A_0 = 1$ mm and gap $d = -2$ mm, respectively. c) Comparison of the theoretical results and simulation results when $k_d/k = 20.62$. d) The displacement distributions of the resonator at different states in vibration. e) The unit cell selection of TENG-MFM. f) The reciprocal lattice of MFM-TENG, the direction chosen as $O \rightarrow \Gamma \rightarrow X \rightarrow O$. g) The dispersion curve and mode shape of TENG-MFM unit cell. Point A shows the first local resonant mode, and the light blue area shows the bandgap region.

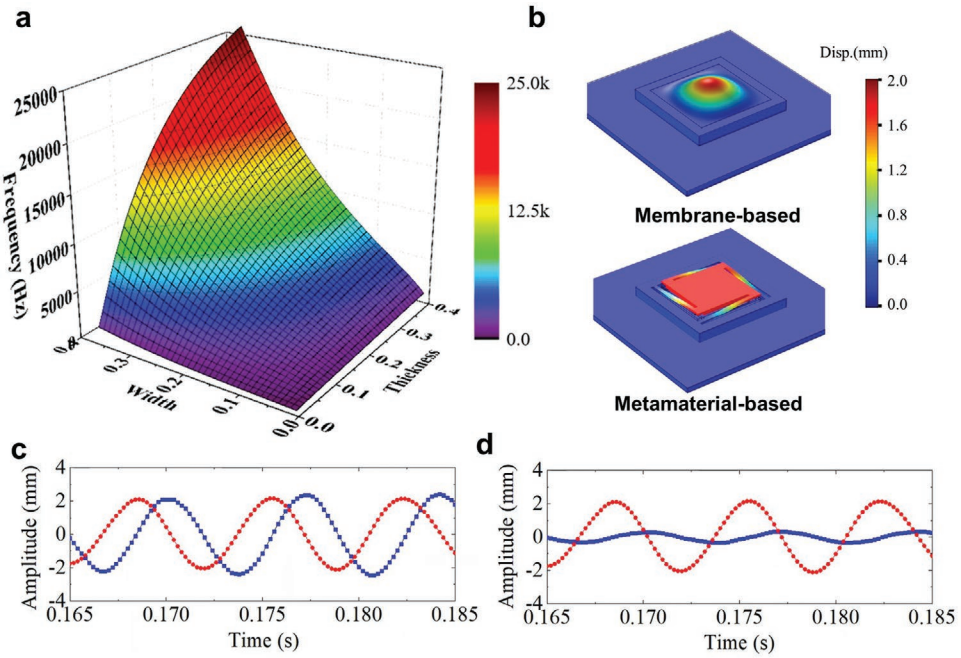

Figure 3. Dynamic response of a unit cell of triboelectric nanogenerator multifunctional metamaterial (TENG-MFM). a) The maximum deflections of the central mass of TENG-MFM under a center force at different frequences. The connecting configurations change with one connection beam. The gap size between adjacent connection beams is 0.05. b) Comparison of the first resonant modes of a membrane-type metamaterial and TENG-MFM at the same excitation frequency of 190 Hz. c) Comparison of the displacement amplitude at the center point of the unit cell of the two types of metamaterials under the same input load. d) Comparation of the displacement amplitude at the points near the unit cell boundary in the two types of metamaterials under the same input loadings.

in subwavelength scales, enabling them to be useful for most engineering applications.

2.3. Results and Discussion

To facilitate the discussion and comparison in the following analysis, we normalize the key parameters as follows: beam width $D = d/l_0$, beam length $L_n = l_n/l_0$, beam number $n = 1$, 2, 3, center resonator length $L_m = l_m/l_0$, plate thickness $T_{t=t/l0}$, the gap between two beams $G_{p=gp}/l_0$, where l_0 is the unit cell size. Thus, we obtain $L_m = 1 - 2n(D + G_p)$ with $L_m \geq 0$, and $L_n = 1 - n(D + G_p)$, and the moment of each connecting beam is $I = \mathrm{D}T_t\,\hat{}\,3/12$ with cross-section area $A = \mathrm{D}T_t$. Additionally, the frequency can be normalized as $\omega = \omega_s/\omega_0$, where $\omega_0 = \sqrt{\frac{EI}{\rho A}}$.

Figure S5 (Supporting Information) shows the maximum amplitude of the central mass in an orthogonal spiral metamaterial with one to three segments in each connecting beam. It is obvious that the working frequency of the TENG-MFM with a one-segment connecting beam increases with the gap size, the beam width, and the plate thickness (Figure S5a–c, Supporting Information). There is an optimal resonant region where only the first-order resonance was considered. Compared with Figure S5d,e,g–i (Supporting Information), we find that the high-order modes will appear with the increase of the number of segments in each connecting beam, i.e., the length of the connecting beam, and the number of high-order modes is equal to the number of the segments in the connecting beams. Moreover, the optimized first-order mode will shift to the low-frequency regions.

Figure 3 presents the dynamic responses of a unit cell of TENG-MFM under a force applied at the bass with different frequences for the structure configurations with one-segment (Figure 3a), connecting beams. In our simulations, the gap size between the adjacent connecting beams is fixed to be 0.5 mm. It can be seen that for a given frequency, the critical width and thickness should be selected to maximize the performance of the TENG-MFM. From the simulation results, we also find that the proposed TENG-MFM has a much better performance in energy harvesting compared with the previous membrane-type metamaterial due to the nearly parallel surface contact and larger contact areas between the two TENG triboelectric layers (Figure 3b–d).

2.4. Experimental Characterization and Evaluation of the MFM

For each TENG-based unit cell, the two triboelectric layers: Al film and PTFE film will have contact-separation interactions under the excited vibrations. In this process, when the suspended PTFE triboelectric layer is oscillated toward the other Al layer, the charge separation is induced at the two surfaces to form a potential difference (**Figure 4**a). Because PTFE is easy to gain electrons while Al is easily to lose electrons, the positive charges will be generated on the Al surface and the negative charges appear on the PTFE surface. Once the PTFE begins to approach to the Al film, the potential difference between two surfaces will gradually decrease, leading to an electron flow from the lower electrode to the upper electrode. When the

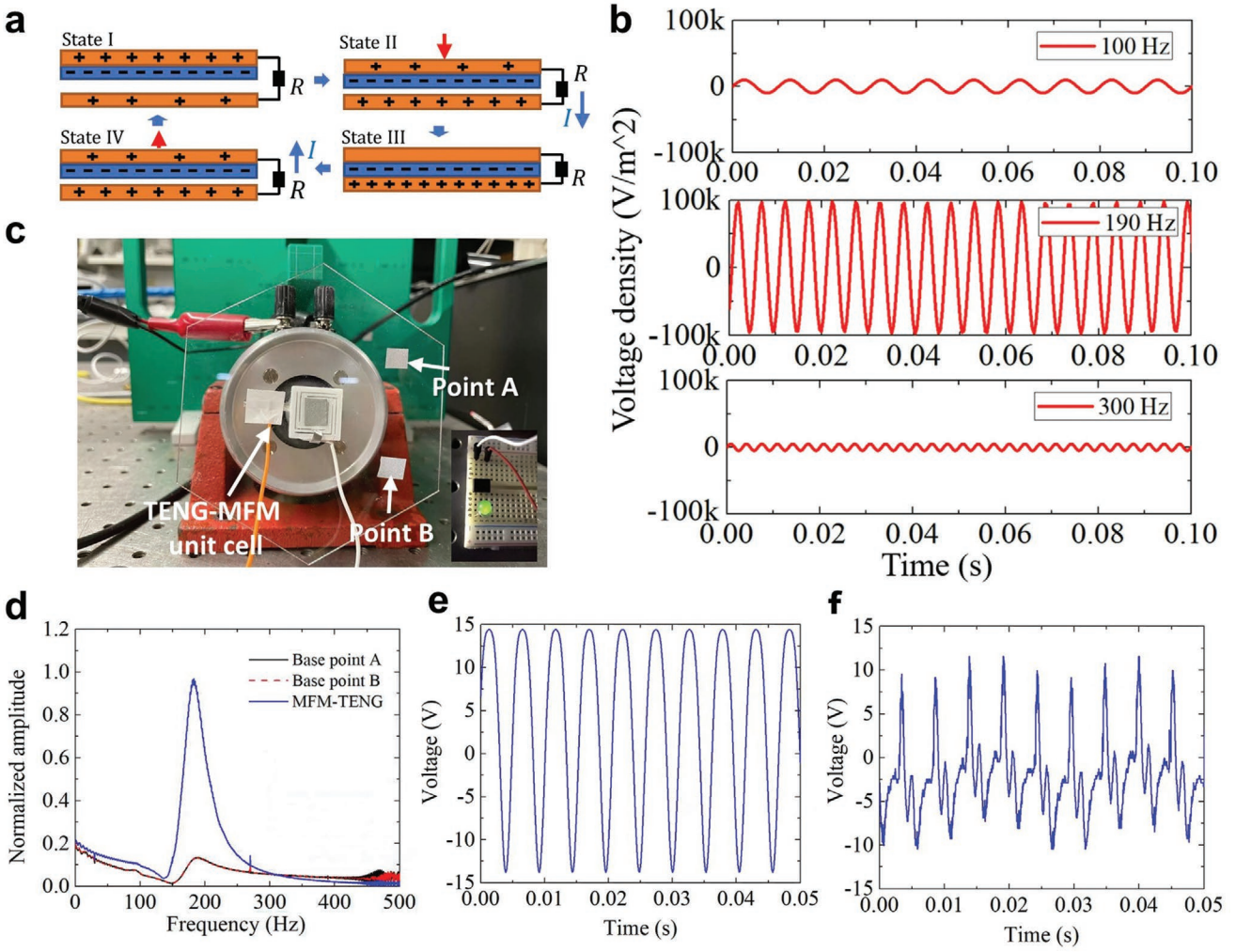

Figure 4. Performance evaluation for the unit cell of triboelectric nanogenerator multifunctional metamaterial (TENG-MFM). a) Schematic of the working principle of the contact-separation mode TENGs. b) Normalized output voltage density of the unit cell under different frequencies: 100, 190, and 300 Hz. c) Experimental setup for the unit cell testing. TENG-MFM is fixed in the center of an acrylic plate, and the reflectors are attached in the center of the unit cell, points A and B to record the vibration signals. d) Normalized amplitude of the unit cell measured at the three points shown in (c). The applied frequency is swept from 20 to 500 Hz. e) The output voltage of the unit cell at 190 Hz, calculated by the numerical model. f) The output voltage of the unit cell at 190 Hz, measured by the experimental test shown in (c).

two triboelectric layers separate from each other, the electrons move back from the upper electrode to the lower electrode. Cyclic contact-separation operations will generate an alternative current between the two electrodes. Figure 4b shows the normalized output voltage density of the unit cell at 100, 190, 300 Hz. It is shown that at resonant excitation frequency, the unit cell consisting of one-segment connecting beams can generate the maximum voltage, thereby the best energy harvesting performance.

To verify the numerical results, we test the unit cell by applying a cycling loading at the resonant frequency onto the specimen in a displacement control manner until it is fully stabled. Figure 4c presents the experimental setup for a unit cell to measure its resonant frequency. The TENG-MFM unit cell is fixed at the center of a rigid plate, and the reflectors are, respectively, attached at the center of the unit cell and the Points A and B to measure the vibration signals. A laser vibrometer is used to capture the vibration of TENG-MFM. The sweep-sine signal from 20 to 500 Hz is selected for the experimental testing. The voltage signal is recorded with an impedance of 100 MΩ. As shown in Figure 4d, the resonant frequency of the designed TENG-MFM should be around 185 Hz. Simulation results indicate that the proposed TENG-MFM unit cell can generate an output voltage of up to 14.5 V when it is excited at the frequency of 190 Hz (Figure 4e). The as-fabricated TENG-MFM unit cell produces an output voltage of about 10 V (Figure 4f), a little smaller than the simulation results due to the induced discrepancy in the fabrication and assembly process of the device. The tested unit cell can successfully lighten a LED through harvesting vibration energy in the experiments (see the inset of Figure 4d). Following the equation: $Q = \int Idt$, the transferred charges of the unit cell of the TENG-MFM can reach 0.04 nC under the excitation frequency of 190 Hz, by integrating the measure positive current in one vibration period (see Figure S10, Supporting Information).

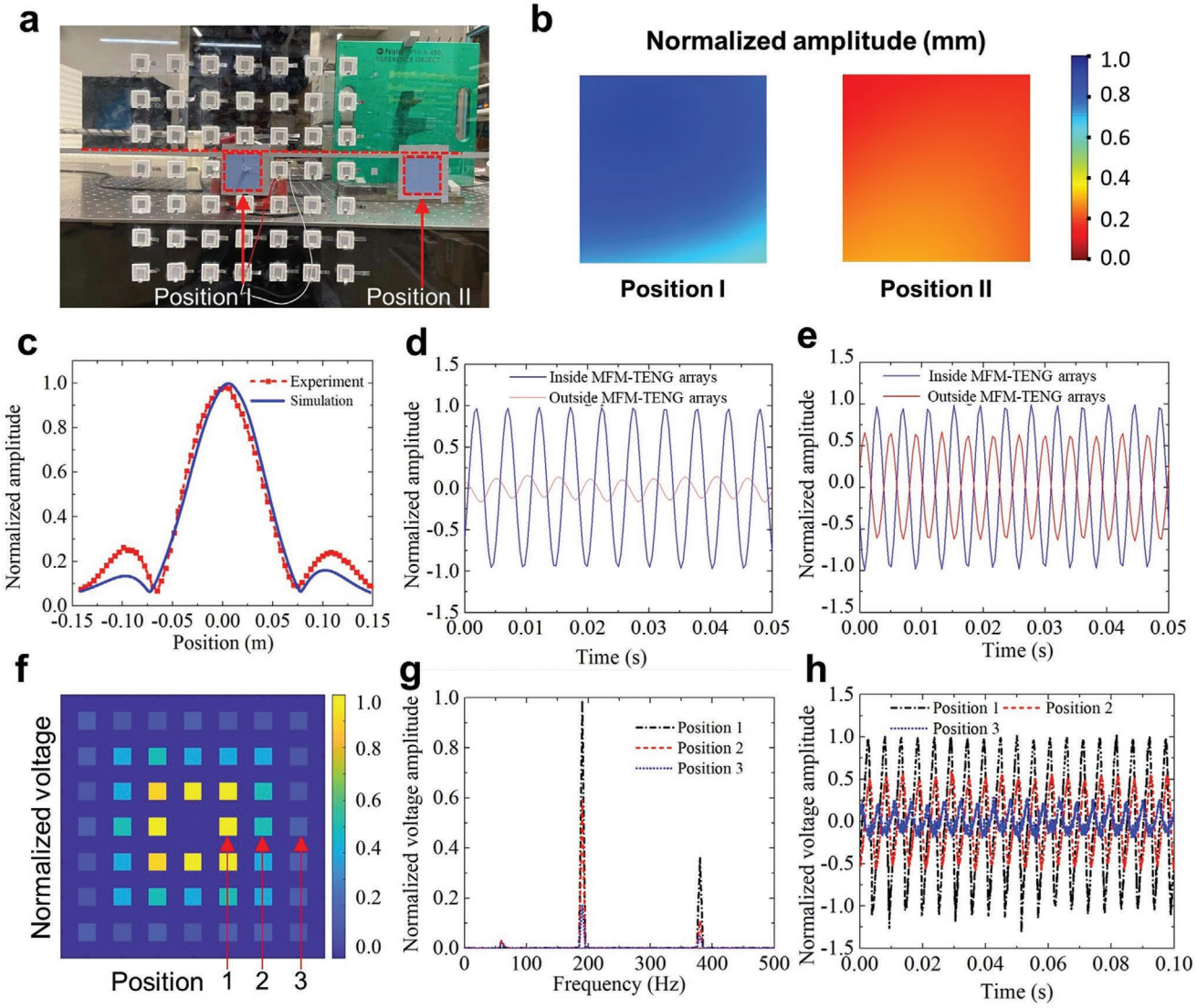

Figure 5. Evaluation of a 2D triboelectric nanogenerator multifunctional metamaterial (TENG-MFM) plate consisting of multiple unit cells. a) Experimental setup for the TENG-MFM plate, capable of self-sensing, self-charging, and vibration suppression. The metamaterial array is attached on a 150 × 100 cm acrylate plate and the shaker source is placed at the center of the arrays. b) Distribution of the normalized vibration amplitude at Position I and Position II marked in (a). c) Comparison of the measured and simulated vibration amplitude along the red dash line across the whole TENG-MFM plate. d) The normalized amplitude varying with time at the bandgap region when excitation frequency is 190 Hz, located inside (Position I) and outside (Position II) of TENG-MFM array. e) The normalized amplitude at inside and outside of TENG-MFM array varying with time at the passingband region when excitation frequency is 250 Hz. f) The normalized voltage distribution over the TENG-MFM array, generated at 190 Hz. g) The normalized voltage at frequency domain, measured at Position 1, Position 2, and Position 3 shown in (f). h) The normalized voltage at time domain, measured at Position 1, Position 2, and Position 3 shown in (f).

We further evaluate the overall performance of a TENG-MFM plate made of 48 unit cells on an acrylate plate. **Figure 5**a and Figure S6 (Supporting Information) present the experimental setup for the testing of the TENG-MFM plate. The unit cells are bonded on a 1.5 × 1.0 m acrylate plate to form a pattern and the excitation source (i.e., a shaker) is aligned with the center of the array. Figure 5b shows the vibration amplitude of the unit cell at the Position I and Position II under the resonant frequency of 190 Hz, indicating that the vibration at Position I is much stronger than that at Position II. In other words, the vibration at Position II is significantly suppressed. This phenomenon is also verified by the amplitudes measured along the red dash line in Figure 5a across the center of the MFM plate (Figure 5c). The peak signal nearby the center source is much stronger than that at the boundary region. Figure 5d,e shows the normalized amplitudes of the TENG-MFM array at the bandgap and passing band regions at 190 and 250 Hz. The TENG-MFM array can transport mechanical energy with little interference when the frequency is in the passband regime and suppress the vibration and harvest mechanical energy when the frequency is in the bandgap regime.

Furthermore, we measure the energy harvesting performance of the TENG-MFM array by recording the output voltages of each unit in the TENG-MFM array (Figure 5f). The internal unit cells will generate larger output voltages than those located along the boundary. Fourier transform is performed to convert the time domain signal to frequency domain for easily visualizing the resonant frequencies. As shown in Figure 5g, at frequency domain the voltage distribution over the TENG-MFM array at the excitation of 190 Hz has a maximum voltage generated at the same resonant excitation frequency. The normalized voltages at the positions 1, 2, and 3 on the TENG-MFM have obvious differences. Similar effects can also be found for other excitation frequencies although the influence may become smaller compared with that at the resonant frequency (Figure S7, Supporting Information). Therefore, we can also use this TENG-MFM array as a self-powered vibration sensor for detecting the vibration frequency. TENG-MFM can identify the bandgap and passband by self-sensing. Figure 5h shows the normalized voltages of TENG-MFM at time domain at Positions 1, 2, and 3 shown in Figure 5f. These observations suggested that the proposed TENG-MFM could be used for multiple functionalities, including vibration isolation/suppression, energy harvesting, and self-powered sensing, which may have great potential for future diagnostic dynamics-related measurements for structural materials and implantable devices for biomedical applications.

3. Conclusions

In summary, we have proposed a new type of MFMs based on TENGs that have the potential to be used for energy harvesting, vibration isolation, and even sensing. The analytical model for the unit cell of the MFM was constructed by considering both mechanical constraints and electrostatic influence of the TENG. Theoretical analyses and experimental verification were performed to reveal the dynamic response of the unit cell and the metamaterial. Experimental results have demonstrated the energy harvesting and wave mitigation performance of TENG-MFM at the low-frequency range. This work provides new designs and analysis tools for designing engineered MFMs for energy harvesting and vibration reduction based on TENGs for interesting applications.

Supporting Information

Supporting Information is available from the Wiley Online Library or from the author.

Acknowledgements

This work was partially supported by NSF (ECCS-2024649), USDA (2021-67021-33998), and USDOT (693JK32050003CAAP). G.L.H. acknowledges the Air Force Office of Scientific Research under Grant No. AF 9550-18-1-0342 and AF 9550-20-0279 with Program Manager Dr. Byung-Lip (Les).

Conflict of Interest

The authors declare no conflict of interest.

Data Availability Statement

The data that support the findings of this study are available from the corresponding authors upon reasonable request.

Keywords

energy harvesting, multifunctional metamaterials, triboelectric nanogenerators, vibration reduction

Received: August 10, 2021
Revised: October 20, 2021
Published online:

[1] B. Banerjee, *An Introduction to Metamaterials and Waves in Composites*, CRC Press, Boca Raton, FL **2011**.
[2] J. B. Pendry, *Phys. Rev. Lett.* **2000**, *85*, 3966.
[3] R. F. Gibson, *Compos. Struct.* **2010**, *92*, 2793.
[4] A. D. B. Ferreira, P. R. Nóvoa, A. T. Marques, *Compos. Struct.* **2016**, *151*, 3.
[5] Z. Liu, X. Zhang, Y. Mao, Y. Y. Zhu, Z. Yang, C. T. Chan, P. Sheng, *Science* **2000**, *289*, 1734.
[6] X. Xu, P. Li, X. Zhou, G. Hu, *Europhys. Lett.* **2015**, *109*, 28001.
[7] R. L. Lincoln, F. Scarpa, V. P. Ting, R. S. Trask, *Multifunct. Mater.* **2019**, *2*, 043001.
[8] K. Yu, N. X. Fang, G. Huang, Q. Wang, *Adv. Mater.* **2018**, *30*, 1706348.
[9] M. Yuan, X. Sheng, Z. Cao, Z. Pang, G. Huang, *Smart Mater. Struct.* **2020**, *29*, 035012.
[10] Y. Y. Chen, M. V. Barnhart, J. K. Chen, G. K. Hu, C. T. Sun, G. L. Huang, *Compos. Struct.* **2016**, *136*, 358.
[11] J. U. Surjadi, L. Gao, H. Du, X. Li, X. Xiong, N. X. Fang, Y. Lu, *Adv. Eng. Mater.* **2019**, *21*, 1800864.
[12] K. Bertoldi, V. Vitelli, J. Christensen, M. Van Hecke, *Nat. Rev. Mater.* **2017**, *2*, 17066.
[13] X. Xu, M. V. Barnhart, X. Li, Y. Chen, G. Huang, *J. Sound Vib.* **2019**, *442*, 237.
[14] X. Xu, M. V. Barnhart, X. Fang, J. Wen, Y. Chen, G. Huang, *Int. J. Mech. Sci.* **2019**, *164*, 105159.
[15] X. Xu, C. Wang, W. Shou, Z. Du, Y. Chen, B. Li, W. Matusik, N. Hussein, G. Huang, *Phys. Rev. Lett.* **2020**, *124*, 114301.
[16] S. Naifar, S. Bradai, C. Viehweger, O. Kanoun, *Measurement* **2017**, *106*, 251.
[17] M. A. Halim, R. Rantz, Q. Zhang, L. Gu, K. Yang, S. Roundy, *Appl. Energy* **2018**, *217*, 66.
[18] S. Mohammadi, A. Esfandiari, *Energy* **2015**, *81*, 519.
[19] Q. Deng, M. Kammoun, A. Erturk, P. Sharma, *Int. J. Solids Struct.* **2014**, *51*, 3218.
[20] W. He, Y. Qian, B. S. Lee, F. Zhang, A. Rasheed, J. E. Jung, D. J. Kang, *ACS Appl. Mater. Interfaces* **2018**, *10*, 44415.
[21] Z. L. Wang, *Mater. Today* **2017**, *20*, 74.
[22] S. Chen, Y. Pang, Y. Cao, X. Tan, C. Cao, *Adv. Mater. Technol.* **2021**, *6*, 2100084.
[23] Y. Pang, Y. Cao, M. Derakhshani, Y. Fang, Z. L. Wang, C. Cao, *Matter* **2021**, *4*, 116.
[24] Y. Pang, S. Chen, J. An, K. Wang, Y. Deng, A. Benard, N. Lajnef, C. Cao, *Adv. Funct. Mater.* **2020**, *30*, 2003598.
[25] Y. Pang, S. Chen, Y. Chu, Z. L. Wang, C. Cao, *Nano Energy* **2019**, *66*, 104131.
[26] S. Chen, Y. Pang, H. Yuan, X. Tan, C. Cao, *Adv. Mater. Technol.* **2020**, *5*, 1901075.

[27] S. Niu, S. Wang, L. Lin, Y. Liu, Y. S. Zhou, Y. Hu, Z. L. Wang, *Energy Environ. Sci.* **2013**, *6*, 3576.
[28] Y. Fu, H. Ouyang, R. B. Davis, *J. Phys. D: Appl. Phys.* **2020**, *53*, 215501.
[29] S. Wang, Y. Xie, S. Niu, L. Lin, Z. L. Wang, *Adv. Mater.* **2014**, *26*, 2818.
[30] M. Ma, Z. Kang, Q. Liao, Q. Zhang, F. Gao, X. Zhao, Z. Zhang, Y. Zhang, *Nano Res.* **2018**, *11*, 2951.
[31] C. Wu, R. Liu, J. Wang, Y. Zi, L. Lin, Z. L. Wang, *Nano Energy* **2017**, *32*, 287.
[32] M. Salauddin, R. M. Toyabur, P. Maharjan, J. Y. Park, *Nano Energy* **2018**, *45*, 236.
[33] Y. Yang, H. Zhang, J. Chen, Q. Jing, Y. S. Zhou, X. Wen, Z. L. Wang, *ACS Nano* **2013**, *7*, 7342.
[34] A. A. Santos, J. D. Hobeck, D. J. Inman, *Smart Mater. Struct.* **2016**, *25*, 115017.
[35] W. Hongjin, M. Qingfeng, F. Wuwei, *Shock and Vibration* **2014**, *2014*, 981053.
[36] J. Shao, D. Liu, M. Willatzen, Z. L. Wang, *Appl. Phys. Rev.* **2020**, *7*, 011405.
[37] G. Xu, X. Li, X. Xia, J. Fu, W. Ding, Y. Zi, *Nano Energy* **2019**, *59*, 154.